# Design of an Adaptive $H_\infty$ Controller for Linear Induction Motor

Keun-Ho Hyun* and In-Hwan Son*

*Dept. of Electrical Engineering, Shinsung College, Dangjin-Gun, Chungnam, Korea
(Tel : +82-41-350-1232,4 ; E-mail : hyunkh@shinsung.ac.kr)

**Abstract :** In this study, an adaptive control scheme with a pre-specified $H_\infty$ property is proposed for the tracking control of linear induction motor (LIM) drive system. Under the influence of uncertainties and external disturbances, by using nonlinear decoupling and parameter tuner, the robust performance control problem is formulated as a nonlinear $H_\infty$ problem and solved by a quadratic storage function. This new design method is able to track the step and several periodic commands with improved performance in face of parameter perturbations and external disturbances. Simulation and experimental results are provided to demonstrate the effectiveness of the proposed adaptive $H_\infty$ controller.

**Keywords :** LIM, adaptive, $H_\infty$, uncertainties, disturbances, linearization, decouple

## 1. INTRODUCTION

The LIM has many advantages such as simple structure, alleviation of gear between motor and the motion devices, reduction of mechanical losses and the size of motion devices, high-speed operation, silence, high-starting thrust force, etc.[1]. Because of the advantages mentioned above, the LIM has been used widely in the field of industrial processes and transportation applications [2]. However, there is strong interaction between the machine process and the direct drive of LIM. Therefore, the drive control system must provide high tracking performance and high dynamic stiffness.

The driving principles of the LIM are similar to the traditional rotary induction motor (RIM), but its control characteristics are more complicated than the RIM, therefore, its mathematical model is difficult to derive completely. Moreover, the dynamic model of the LIM can be modified from the dynamic model of the RIM at certain low speeds since the LIM can be visualised to unroll a rotary induction motor. Thus, many decoupled control techniques in RIM can be adopted to decouple the dynamics of the trust force and the flux amplitude of the LIM [3]. The motivation of this study is to design a suitable control scheme to confront the uncertainties existing in the incomplete dynamic model of the LIM.

During the past decade, the $H_\infty$ control strategy has been widely celebrated for its robustness in counteracting uncertainty perturbations and external disturbances. consequently, some applications of this approach to various plants such as DC motors [4], switching converters [5] and aircraft [6] have been published. The main point of the $H_\infty$ control is to synthesize a feedback law that renders the closed-loop system to satisfy a prescribed $H_\infty$ -norm constraint which representing desired stability or tracking requirements. An $H_\infty$ controller design with adaptive mechanism is developed for a nonlinear system under both parameter uncertainties and external load disturbance.

Since adaptive control systems are inherently nonlinear, the derivation of the proposed controller is relied on nonlinear $H_\infty$ control theory [7]. By choosing a quadratic storage function, the solution of the adaptive $H_\infty$ problem has a simple structure and is suitable for digital realization.

In this study, an adaptive $H_\infty$ controller is designed to control the position of a mover of the LIM for the tracking of periodic step, sinusoidal references. The considered uncertainties are variation of mover mass, friction coefficient and unknown external disturbance force, which are the major concerns in motion control applications.

## 2. NONLINEAR DECOUPLE CONTROL

The dynamic model of the LIM is modified from the traditional model of a 3-phase, Y-connected induction motor in a d-q stationary reference frame and can be described by the following differential equations [2].

$$\dot{i}_{qs} = -\left(\frac{R_s}{\sigma L_s} + \frac{1-\sigma}{\sigma T_r}\right)i_{qs} - \frac{L_m \pi}{\sigma L_s L_r \tau}v\lambda_{dr}$$
$$+ \frac{L_m}{\sigma L_s L_r T_r}\lambda_{qr} + \frac{1}{\sigma L_s}V_{qs} \qquad (1)$$

$$\dot{i}_{ds} = -\left(\frac{R_s}{\sigma L_s} + \frac{1-\sigma}{\sigma T_r}\right)i_{ds} + \frac{L_m}{\sigma L_s L_r T_r}\lambda_{dr}$$
$$+ \frac{L_m \pi}{\sigma L_s L_r \tau}v\lambda_{qr} + \frac{1}{\sigma L_s}V_{ds} \qquad (2)$$

$$\dot{\lambda}_{qr} = \frac{L_m}{T_r}i_{qs} + n_p\frac{\pi}{\tau}v\lambda_{dr} - \frac{1}{T_r}\lambda_{qr} \tag{3}$$

$$\dot{\lambda}_{dr} = \frac{L_m}{T_r}i_{ds} - \frac{1}{T_r}\lambda_{dr} - n_p\frac{\pi}{\tau}v\lambda_{qr} \tag{4}$$

$$F_e = K_f(\lambda_{dr}i_{qs} - \lambda_{qr}i_{ds}) = M\dot{v} + Dv + F_L \tag{5}$$

where $T_r = L_r/R_r$, $\sigma = 1 - (L_m^2/L_sL_r)$, $K_f = (3/2)n_p(\pi L_m/\tau L_r)$ and

$R_s$ = primary resistance per phase [Ω]
$R_r$ = secondary resistance per phase [Ω]
$L_m$ = magnetising inductance per phase [H]
$L_s$ = primary inductance per phase [H]
$L_r$ = secondary inductance per phase [H]
$v$ = mover linear velocity [m/sec]
$\lambda_{dr}$ = d-axis secondary flux [Wb]
$\lambda_{qr}$ = q-axis secondary flux [Wb]
$i_{ds}$ = d-axis primary current [A]
$i_{qs}$ = q-axis primary current [A]
$V_{ds}$ = d-axis primary voltage [V]
$V_{qs}$ = q-axis primary voltage [V]
$T_r$ = secondary time constant
$\sigma$ = leakage coefficient
$F_e$ = electromagnetic force [N]
$K_f$ = force constant [N/V]
$F_L$ = load disturbance [N]
$M$ = total mass of the moving element [kg]
$D$ = viscous friction coefficient [kg/sec]
$\tau$ = pole pitch [m]
$n_p$ = number of pole pairs

The secondary flux amplitude is defined as

$$\lambda_r = \sqrt{(\lambda_{dr})^2 + (\lambda_{qr})^2} \tag{6}$$

and using Eq.(3) and Eq.(4), the time derivative of $\lambda_r$ can be derived as follows:

$$\dot{\lambda}_r = -\frac{\lambda_r}{T_r} + \frac{L_m(i_{ds}\lambda_{dr} + i_{qs}\lambda_{qr})}{T_r\lambda_r} \tag{7}$$

From Eq.(5), the LIM motion dynamics can be expressed as

$$\dot{v} = -\frac{D}{M}v + \frac{K_f}{M}(\lambda_{dr}i_{qs} - \lambda_{qr}i_{ds}) - \frac{F_L}{M} \tag{8}$$

In the LIM dynamics described by Eq.(7) and (8), $i_{ds}$ and $i_{qs}$ are the control inputs, and $\lambda_r$ and $v$ are the system outputs. Thus, the LIM dynamic is a coupled system. Since there are no direct relations between the outputs and inputs, it is difficult to design the control inputs $i_{ds}$ and $i_{qs}$ so that the system outputs $\lambda_r$ and $v$ can track the desired trajectories accurately. Therefore, the nonlinear state feedback theory is used to eliminate this

coupling relationship between the control inputs $i_{ds}$, $i_{qs}$ and the system outputs $\lambda_r$, $v$ to simplify the design of the position controller. Two new control inputs $u_d$ and $u_q$ are chosen as follows

$$\begin{bmatrix} u_d \\ u_q \end{bmatrix} = \frac{1}{\lambda_r}\begin{bmatrix} \lambda_{dr} & \lambda_{qr} \\ -\lambda_{qr}\lambda_r & -\lambda_{dr}\lambda_r \end{bmatrix}\begin{bmatrix} i_{ds} \\ i_{qs} \end{bmatrix} \tag{9}$$

From Eq.(9), the feedback linearization controller can be derived as follows:

$$\begin{bmatrix} i_{ds} \\ i_{qs} \end{bmatrix} = \frac{1}{\lambda_r^2}\begin{bmatrix} \lambda_{dr}\lambda_r & -\lambda_{qr} \\ \lambda_{qr}\lambda_r & -\lambda_{dr} \end{bmatrix}\begin{bmatrix} u_d \\ u_q \end{bmatrix} \tag{10}$$

Substituting Eq.(10) into Eq.(7) and Eq.(8), the decoupled equations can be obtained as follows

$$\dot{\lambda}_r = -\frac{\lambda_r}{T_r} + \frac{L_m}{T_r}u_d \tag{11}$$

$$\dot{v} = -\frac{D}{M}v + \frac{K_f}{M}u_q - \frac{F_L}{M} \tag{12}$$

Thus, the new inputs $u_d$ and $u_q$ can be used to control the secondary flux amplitude and mover position, respectively. The nonlinear decoupled LIM drive system consists of a ramp-comparison current-controlled pulse-width modulated (PWM) voltage source inverter (VSI), a feedback linearization controller, two co-ordinate translators, a speed-control loop and a position-control loop, The LIM used in this drive system is a 3-phase Y-connected tow-pole 3[kW], 60[Hz], 220[V] type as depicted at Fig.1.
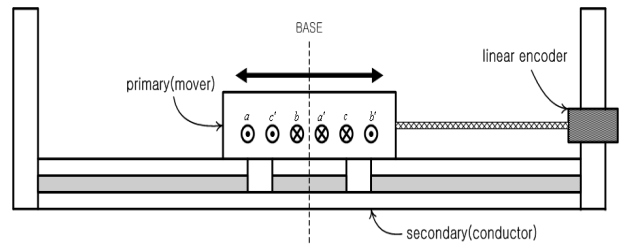


Fig.1 Structure of an experimental LIM

The detailed parameters of the LIM are

$u_d$ = 2.35[A], $R_s$ = 5.3685[Ω],
$R_r$ =3.5315[Ω], $\tau$ = 27[mm], $\qquad$ (13)
$L_m$ = 24.19[mH], $L_s = L_r$ = 28.46[mH]

where $u_d$ is the flux current command. By use of the nonlinear decoupled technique and with the fact that the electrical time constant is much smaller than the mechanical time constant, the LIM drive system can be reasonably represented by the control system block diagram shown in Fig.2, in which

$$F_e = K_f u_q \qquad (14)$$

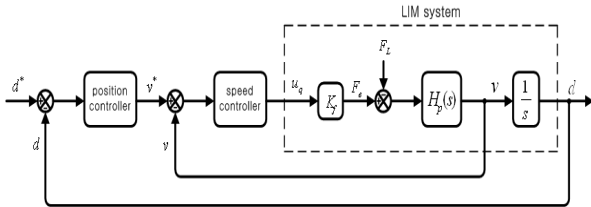$$H_p(s) = \frac{1}{Ms+D} = \frac{b}{s+a} \qquad (15)$$



Fig.2 Block diagram of LIM control system

where $u_q$ is the thrust command voltage. The curve fitting technique based on step response is applied to fine the drive model off-line at the nominal case ($F_L = 0$). The results are (on a scale of 1.5915[m/sec/V])

$$K_f = 148.35[\text{N/V}], \ a=12.965, \ b= 0.226,$$
$$\overline{M} = 2.79[\text{kg}] = 4.4245[\text{N·sec/V}], \qquad (16)$$
$$\overline{D} = 36.0455[\text{kg/sec}] = 57.3664[\text{N/V}]$$

The '‾' symbol represents the system parameters in the nominal condition.

## 3. ADAPTIVE $H_\infty$ CONTROL DESIGN

To counteract the effect of parameter variations and external disturbances, an adaptive tracking control scheme with a guaranteed $H_\infty$ performance is proposed. It consists of finding a static or dynamic feedback controller such that $H_\infty$-norm of the closed-loop transfer function is less than a given positive number under the constraint that the closed-loop system is internally stable. To apply this method, the LIM position tracking problem must be formulated into an equivalent $H_\infty$ control problem in which robust performance requirements in terms of $H_\infty$-norm constraints on the tracking error dynamics.

By rewriting Eq.(12), the dynamic equation of the LIM drive system can be put into the following form.

$$\ddot{d} = -\frac{D}{M}\dot{d} + \frac{K_f}{M}u_q - \frac{F_L}{M} \qquad (17)$$

where $d$ is the mover position of the LIM. Define the tracking error vector as follows

$$\boldsymbol{E} = [d-d^* \ \ v-v^*]^T = [e \ \ \dot{e}]^T \qquad (18)$$

where $e$ is the tracking error of mover position, and $d^*$ and $v^*$ represent the desired mover position

and speed, respectively. Since the plant parameters $M$ and $D$ are uncertain, $\hat{M}$ and $\hat{D}$ are denoted as their estimated, and the corresponding matrices $\boldsymbol{\psi} = [D \ M]^T$ and $\hat{\boldsymbol{\psi}} = [\hat{D} \ \hat{M}]^T$ are defined. In oder to obtain the tracking error dynamic for arbitrary input command, a preliminary feed-forward term.

$$u_q = \frac{1}{K_f}(\hat{D}\dot{d} + \hat{M}\ddot{d}^* - \hat{M}\boldsymbol{KE} + \hat{M}u) \qquad (19)$$

is first applied, where $\boldsymbol{K} = [k_1 \ k_2]$ with $k_1$ and $k_2$ being any positive constants, and $u$ is the outer-loop control to be further specified later. By substituting Eq.(19) into Eq.(17), it can be obtained that

$$\hat{M}(\ddot{d} - \ddot{d}^*) = \hat{M}(\tilde{\boldsymbol{\psi}}^T\boldsymbol{\phi} - \boldsymbol{KE} + u) - F_L \qquad (20)$$

where $\tilde{\boldsymbol{\psi}} = \hat{\boldsymbol{\psi}} - \boldsymbol{\psi} = [\hat{D}-D \ \ \hat{M}-M]^T$, $\boldsymbol{\phi} = \hat{M}^{-1}[\dot{d} \ \ \ddot{d}]$. Thus, using the definition of Eq.(18), Eq.(20) can be rewritten as

$$\ddot{e} = \tilde{\boldsymbol{\psi}}^T\boldsymbol{\phi} - \boldsymbol{KE} - \hat{M}^{-1}F_L + u \qquad (21)$$

The error dynamics equation (21) can be described by the state-space representation

$$\begin{bmatrix} \dot{e}_1 \\ \dot{e}_2 \end{bmatrix} = \begin{bmatrix} 0 & 1 \\ -k_2 & -k_1 \end{bmatrix}\begin{bmatrix} e_1 \\ e_2 \end{bmatrix} + \begin{bmatrix} 0 \\ 1 \end{bmatrix}\tilde{\boldsymbol{\psi}}^T\boldsymbol{\phi} + \begin{bmatrix} 0 \\ -\hat{M}^{-1} \end{bmatrix}w + \begin{bmatrix} 0 \\ 1 \end{bmatrix}u \qquad (22)$$

where $e_1 = e$, $e_2 = \dot{e}$ and $w = F_L$. In order to achieve a zero steady-state error, an integral action

$$\zeta = \int_0^t e \ dt = \int_0^t e_1 \ dt \qquad (23)$$

is introduced and together with Eq.(22), the augmented error dynamics can be expressed as

$$\dot{\boldsymbol{x}} = \boldsymbol{Ax} + \boldsymbol{B}_1(\tilde{\boldsymbol{\psi}}^T\boldsymbol{\phi} + u) + \boldsymbol{B}_2(\hat{\boldsymbol{\psi}})w \qquad (24)$$

where $\boldsymbol{x} = \begin{bmatrix} e_1 \\ e_2 \\ \zeta \end{bmatrix}$, $\boldsymbol{A} = \begin{bmatrix} 0 & 1 & 0 \\ -k_2 & -k_1 & 0 \\ 1 & 0 & 0 \end{bmatrix}$, $\boldsymbol{B}_1 = \begin{bmatrix} 0 \\ 1 \\ 0 \end{bmatrix}$, $\boldsymbol{B}_2(\hat{\boldsymbol{\psi}}) = \begin{bmatrix} 0 \\ -\hat{M}^{-1} \\ 0 \end{bmatrix}$.

Let the penalty variable $\boldsymbol{z}$ be chosen as

$$\boldsymbol{z} = \boldsymbol{Cx} + \boldsymbol{D}u \ \text{with} \ \boldsymbol{C} = \begin{bmatrix} c & 0 & 0 \\ 0 & 0 & 0 \end{bmatrix}, \ \boldsymbol{D} = \begin{bmatrix} 0 \\ d \end{bmatrix} \qquad (25)$$

where $c$ and $d$ are weighting constants, which have to be determined so that the desired performance specifications are achieved. Now, for the augmented error Eq.(24), the objective is to find a parameter-tunable controller of the form as $\dot{\hat{\boldsymbol{\psi}}} = \alpha(\boldsymbol{x}, \hat{\boldsymbol{\psi}})$, $u = \beta(\boldsymbol{x}, \hat{\boldsymbol{\psi}})$ so that the resulting closed-loop system

$$\dot{\boldsymbol{x}} = \boldsymbol{Ax} + \boldsymbol{B}_1(\tilde{\boldsymbol{\psi}}^T\boldsymbol{\phi} + \beta(\boldsymbol{x}, \hat{\boldsymbol{\psi}})) + \boldsymbol{B}_2(\hat{\boldsymbol{\psi}})w \qquad (26)$$

$$\dot{\hat{\boldsymbol{\psi}}} = \alpha(\boldsymbol{x}, \hat{\boldsymbol{\psi}}) \qquad (27)$$

$$z = Cx + D\beta(x, \hat{\psi}) \tag{28}$$

is stable and the $H_\infty$-norm constraint

$$\int_0^\infty \|z(t)\|^2 dt \leq \epsilon \int_0^\infty \|w(t)\|^2 dt \tag{29}$$

is satisfied for as small a value of $\epsilon$ as possible. Moreover, when $w = 0$ the asymptotic tracking is achieved, i.e. $\lim_{t \to \infty} e_1(t) = 0$. The value of $\epsilon$ in Eq.(29) stands for a measure of the effect of the disturbance $w$ on the penalty variable $z$. From the definition of $z$ in Eq.(29), it is easy to realize that a smaller value of $\epsilon$ will result in better tracking performance. As a summary, the resulting adaptive $H_\infty$ control problem subject to the plant in Eq.(24) is depicted in Fig.3.
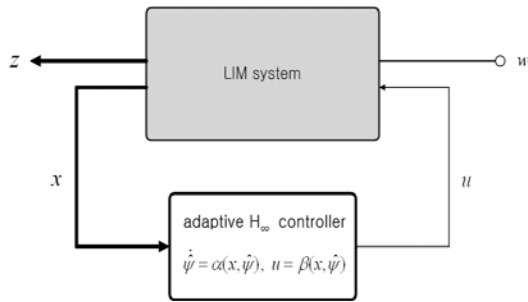


Fig.3 Adaptive $H_\infty$ control problem

In adaptive systems, under the influence of unmodelled dynamics or external disturbances the parameter-drifting phenomenon may occur. A common method to eliminate this phenomenon is to project the parameter estimates into a bounded set. Hence it is assumed that the real parameter vector $\psi$ falls into a known bounded cube $\Omega$. Let $\dot{\Omega}$ and $\delta\Omega$ denote the interior and boundary of the set $\Omega$, respectively. The symbol $N_{\hat{\psi}}$ represents the vector normal to $\delta\Omega$ at $\hat{\psi}$. Since a projective action in the adaptive law will be used to confine the parameters in the set $\Omega$, it can then be easily checked that there exists a constant bounding matrix $G$ such that, for all $\hat{\psi} \in \Omega$, the following inequality holds.

$$B_2(\hat{\psi})B_2(\hat{\psi})^T \leq GG^T \tag{30}$$

Next, the nonlinear $H_\infty$ control theory is applied to derive the adaptive $H_\infty$ controller.

**Theorem 1.** Suppose that the Riccati inequality at given a positive constant $\epsilon > 0$

$$A^T P + PA - \frac{1}{\sigma^2} PB_1^T P + \frac{1}{\epsilon^2} PGG^T P + C^T C \leq 0 \tag{31}$$

has a solution $P > 0$. Then the adaptive law

$$\dot{\theta} = -\Gamma\phi B_1^T Px, \quad \Gamma = diag[\gamma_1 \ \gamma_2] > 0 \tag{32}$$

$$\dot{\hat{\psi}} = \begin{cases} \dot{\theta} & \text{if } \hat{\psi} \in \dot{\Omega} \text{ or } (\hat{\psi} \in \partial\Omega \text{ and } \dot{\theta} \cdot N_{\hat{\psi}} < 0) \\ 0 & \text{if } \hat{\psi} \in \partial\Omega \text{ and } \dot{\theta} \cdot N_{\hat{\psi}} > 0 \end{cases} \tag{33}$$

and control input

$$u = -\frac{1}{\sigma^2} B_1^T Px \tag{34}$$

can stabilize the closed-loop system in Eq.(26)~(28) and the $H_\infty$ tracking performance in Eq.(29) is also achieved.

**Proof.** Selecting the storage function to be

$$V(x, \tilde{\psi}) = x^T Px + \tilde{\psi}^T \Gamma^{-1} \tilde{\psi} \tag{35}$$

and taking its derivative with respect to time, one can obtain

$$\dot{V}(x, \tilde{\psi}) = 2\dot{x}^T Px + 2\dot{\tilde{\psi}}^T \Gamma^{-1} \tilde{\psi} \tag{36}$$

Recall that $\tilde{\psi} = \hat{\psi} - \psi = [\hat{D} - D \quad \hat{M} - M]^T$, the projective action in Eq.(33) ensures that

$$(\dot{\hat{\psi}} - \dot{\theta})^T \Gamma^{-1} \tilde{\psi} = \sum_{i=1}^2 (\dot{\hat{\psi}}_i - \dot{\theta}_i) \Gamma_i^{-1} \tilde{\psi}_i \leq 0 \tag{37}$$

Next, proceed to derive that the $H_\infty$ inequality (29) is achieved by using Eq.(30), (32), (34) and (37), and the completion of the squares in the form of inequality.

$$\dot{V} \leq \sigma^2 \left\| u + \frac{1}{\sigma^2} B_1^T Px \right\|^2 - \epsilon^2 \left\| w - \frac{1}{\epsilon^2} B_2^T Px \right\|^2 - z^T z + \epsilon^2 w^2 \tag{38}$$

Choosing $u$ as the one given in Eq.(34), and integrating the above inequality both sides from 0 to $T$ gives

$$\int_0^T (z^T z - \epsilon^2 w^2) dt \leq -\int_o^T \epsilon^2 \left\| w - \frac{1}{\epsilon^2} B_2^T Px \right\|^2 dt + V(0) - V(T)$$

$$\text{for } any \ T > 0 \tag{39}$$

Since $V(0) = 0$, the asymptotic tracking when the disturbance $w$ vanishes can be shown along the usual Lyapunov argument. Indeed, consider the storage function $V$ in Eq.(35) as a Lyapunov function candidate. Note that for $w = 0$, Eq.(38) becomes

$$\dot{V}(x, \tilde{\psi}) \leq -x^T C^T Cx \leq 0 \tag{40}$$

This proves that the unforced closed-loop system is stable. Furthermore, from Lasalle's invariance principle [8] and the fact that $x^T C^T Cx = \epsilon^2 e_1^2$, it is concluded that $\lim_{t \to \infty} e_1(t) = 0$ and this completes the proof.

## 4. SIMULATION AND EXPERIMENT

To investigate the effectiveness of the proposed adaptive $H_\infty$ controller, four cases with parameter variations and external load disturbance are considered here :

Case I : $M = \overline{M}, \ D = \overline{D}, \ F_L = 0$

Case II : $M = 4 \times \overline{M}, \ D = 2 \times \overline{D}, \ F_L = 0$

Case III : $M = \overline{M}, \ D = \overline{D}, \ F_L = 2.0[N]$

Case IV : $M = 4 \times \overline{M}, \ D = 2 \times \overline{D}, \ F_L = 2.0[N]$

where $F_L$ will be applied at 5~15[sec] in CASE III and CASE IV. Moreover, a 3rd-order transfer function of the following form is chosen as the reference model for the periodic step input as $\dfrac{14000}{s^3 + 90s^2 + 2000s + 14000}$. In addition, the design parameters of the adaptive $H_\infty$ controller are given as $c = d = 3, \ \gamma_1 = \gamma_2 = 0.05, \ k_1 = k_2 = 2, \ \sigma = 0.5, \ \epsilon = 0.1$ and $\boldsymbol{G} = diag[0 \ 10 \ 0]$.

Simulation was carried out using CEMTool and sampling interval are set to be 0.5[msec]. Fig.4~7 represent the simulation results for CASE I~IV and display the reference signal $(d^*)$ vs mover position $(d)$ and control effort $(u_q)$, respectively. Mover positions are very well track the reference signal at all cases, however, control efforts are all different according to the existence of parameter variations$(M, D)$ and load disturbance$(F_L)$. Fig.8 and Fig.9 represent tracking error and estimation value of parameter variations in CASE IV, respectively, and its value are smaller or converge to constant values as time elapsed. Especially, tracking error will be zero due to the insertion of integral action $\zeta$ in Eq.(23).

Experimental studies were performed to confirm the simulated results and carried out as Fig.10. The control algorithm are implemented by Turbo C language and DSP(TMS320C32) are used in digital realization. Fig.11 is the results of experiment with $F_L$. The results are almost same as of simulation except a minutely vibration due to the effect of external and measurement noise. The effects of parameter variations nearly do not exist due to the precisely settings of parameter $M$ and $D$.

## 5. CONCLUSIONS

This study has successfully demonstrated the design, stability analysis and implementation of an adaptive H∞ controller for the position control of the mover of an LIM drive system. The curve fitting technique and feedback linearization were used to decouple the thrust force and the flux amplitude of the LIM. By choosing a adequate quadratic storage function, a simple adaptive law in companion with a state feedback term has been theoretically shown to desired $H_\infty$ performance for the tracking of periodic command signals. Unlike usual $H_\infty$ control design, the control scheme presented here introduces a integral action to achieve perfect tracking of periodic commands. Experimental studies were performed to confirm the simulated results.

## REFERENCES

[1]  Takahashi.I and Ide.Y, "Decoupling control of thrust and attractive force of a LIM using a space vector control inverter", IEEE Trans. on Industry Applications, 1993, 29(1), pp.161-167

[2]  Bucci.G, Meo.S, Ometto.A and Scarano.M, "The control of LIM by a generalization of standard vector techniques", Proceedings of IEEE IAS, 1994, pp.623-626

[3]  F.J.Lin and C.C.Lee, "Adaptive backstepping control for linear induction motor drive to track periodic references", IEE Proceedings of Electric Power Applications, 2000, Vol.147, No.6, pp.449-458

[4]  Attaianese.C, Perfetto.A and Tomasso.G, "Robust position control of DC drives by means of $H_\infty$ controllers", IEE Proceedings of Electric Power Applications, 1999, Vol.146, No.4, pp.391-396

[5]  Ioannidis.G.C, and Manidas.S.N, "$H_\infty$ loop-shaping control scheme for the buck converter and their evaluation using $\mu$ synthesis", IEE Proceedings of Electric Power Applications, 1999, 146(2), pp.237-246

[6]  Jonckheere.E.A and Yu.G.R, "Propulsion control of crippled aircraft by $H_\infty$ model matching", IEEE Trans. on Control Systems Technology, 1999, 7(2), pp.142-159

[7]  Michael.G and David.J.N, "*Linear robust control*", 1995, Prentice Hall

[8]  Narendra.K and Annasawanny.A, "*Stable adaptive Systems*", 1989, Prentice Hall
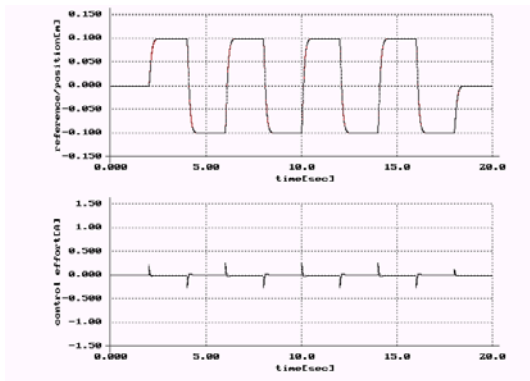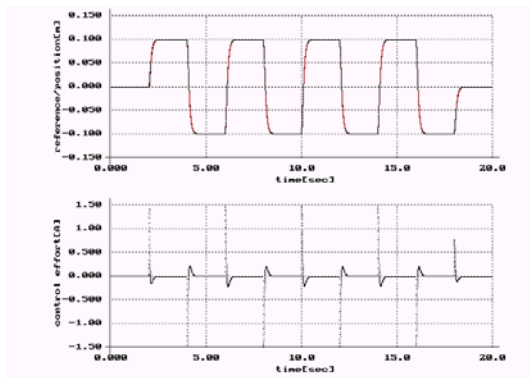
Fig.4 Simulation results for CASE I
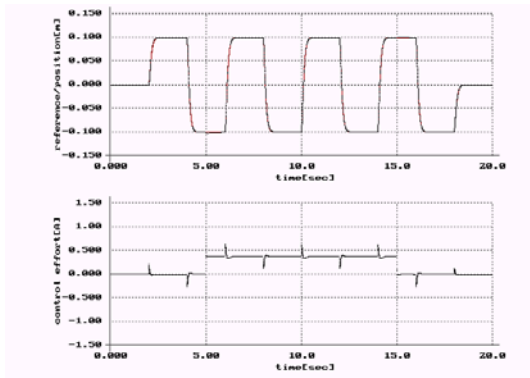


Fig.5 Simulation results for CASE II



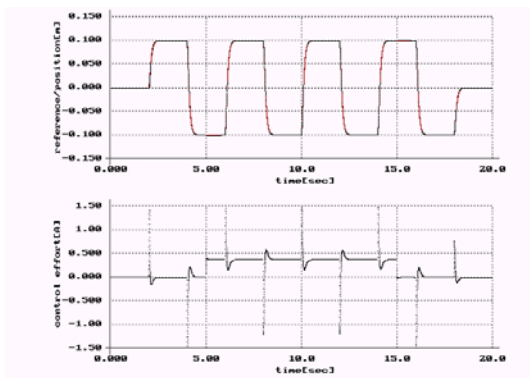Fig.6 Simulation results for CASE III

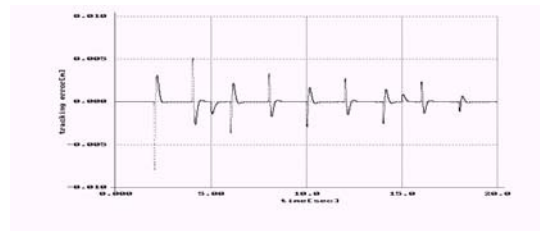

Fig.7 Simulation results for CASE IV



Fig.8 Tracking error for CASE IV



Fig.9 Estimation value of $M$ and $D$ for CASE IV
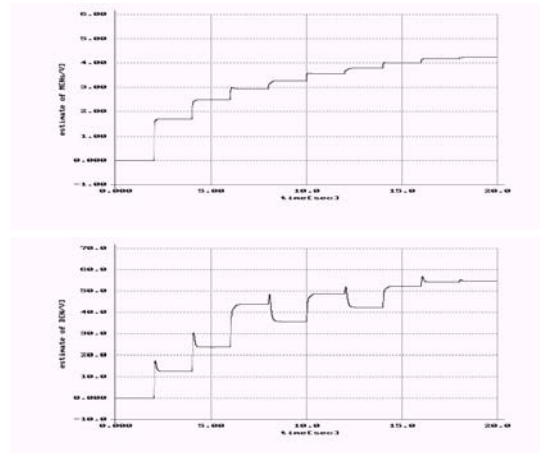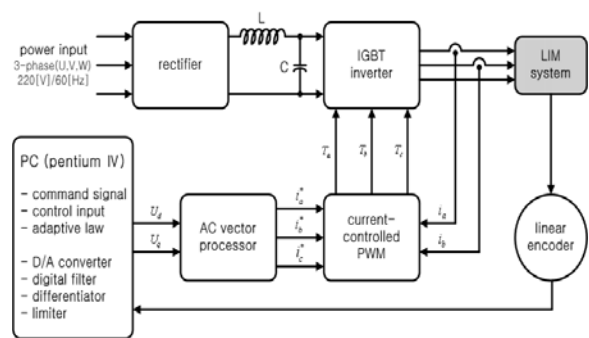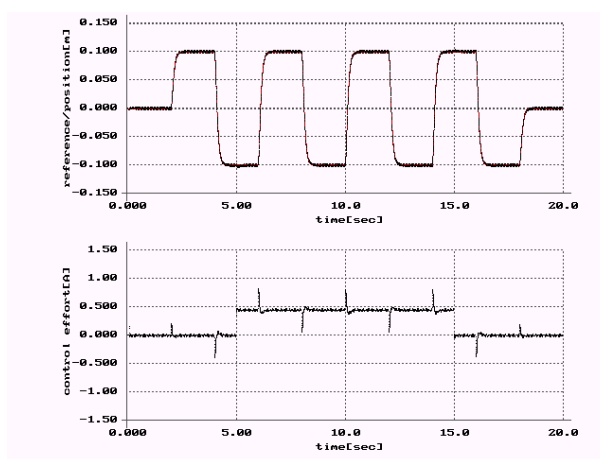


Fig.10 Hardware configuration for LIM drive system



Fig.11 Experimental results with $F_L$